Characterization of the $^1D^e$ autodetaching resonance in H$^-$ and D$^-$

D. C. Rislove,[1] Charlie E. M. Strauss,[2] H. C. Bryant,[1] M. S. Gulley,[2] David J. Funk,[2] Xin Miao Zhao,[3] and W. A. Miller[1]

[1]*Physics and Astronomy, University of New Mexico, Albuquerque, New Mexico 87131*
[2]*Los Alamos National Laboratory, P.O. Box 1663, Los Alamos, New Mexico 87545*
[3]*Cirrus Logic, Incorporated, 4210 South Industrial Drive, Austin, Texas 78744*

We have measured the hydrogen-deuterium isotope shift in the energy of the lowest $^1D^e$ autodetaching resonance in the two-photon absorption spectrum of H$^-$. The $^1D^e$ resonance in negative deuterium lies 2.0 ± 0.5 meV, with a possible systematic error of 0.4 meV, above the corresponding resonance in negative hydrogen when measured with respect to the ion ground state. From the isotope shift, we obtain a mass polarization of 2.4 ± 1.1 meV, with a possible systematic error of 0.8 meV, for the $^1D^e$ in H$^-$ under the assumption that the Fano shape parameters, q, for the two isotopes are the same. Recent theoretical calculations give the mass polarization for this resonance in H$^-$ as -0.1 meV. The generalized absolute cross section of two-photon absorption at the peak of the $^1D^e$ is found to be $(3.2^{+1.8}_{-1.2})\times 10^{-49}$ cm^4 s. The measured asymmetry parameters β_2 and β_4 of the photodetachment process are 1.9 ± 1.2 and 2.21 ± 0.45, respectively, consistent with a pure D-wave distribution. Upper bounds on the second recursion of the lowest $^1S^e$ resonance and three-photon excess photon detachment are 2.8×10^{-49} cm^4 s and 3.1×10^{-78} cm^6 s^2, respectively. [S1050-2947(98)07509-X]

PACS number(s): 32.70.Jz, 31.25.Jf, 32.80.Wr

I. INTRODUCTION

The negative ion of hydrogen (H$^-$), because of its relative simplicity, has long been an important laboratory for the study of electron-electron correlations. Understanding this elementary three-body Coulomb problem, for which the electron-electron interaction is as strong as the electron-nucleus interaction, is a critical first step toward the elucidation of the more complex atomic structures. In this paper we report the results of an experiment designed to characterize the dynamics of the electron-electron interaction in a doubly excited H$^-$ state. We compare measurements on this ion for which the nucleus is a proton with those for which the nucleus is a deuteron. Isotopic shifts provide a way to study correlations in the electron momenta.

There are no singly excited states in negative hydrogen. The ephemeral doubly excited states decay principally by autoionization. Since they are embedded in the continuum and can be formed in electron-neutral-atom collisions as well as by photoexcitation, the doubly excited states are often termed ''autodetaching resonances.'' The spectra of the negative ions of the isotopes of hydrogen differ in subtle ways that reflect the properties of the nuclei. We have chosen as the principal subject of our study the $^1D^e$ state just below the $N=2$ threshold in electron-hydrogen scattering, which we excite from the ground state of H$^-$ using two-photon absorption.

Two-photon spectroscopy techniques developed by Stinz *et al.* [1] made possible high-resolution studies of the lowest $^1D^e$. More recent measurements accurately determined the $^1D^e$ resonance parameters in both H$^-$ and D$^-$ [2]. Most of the isotope shift of the resonance energy can be accounted for using the known isotope shifts of both the electron affinity of H$^-$ and the binding energy of H^0 (Fig. 1). Any remaining isotope shift is the result of a mass polarization effect, which directly reflects the two-electron momenta correlations. The large relative mass difference between H$^-$ and D$^-$ results in an isotope shift that can be easily resolved in our experiment.

Two-photon excitation of the $^1D^e$ is in itself a physically interesting process, and several parameters, including the electron-autodetachment angular asymmetries and the generalized absolute cross section, are determined from our data. The $^1S^e$ symmetry of the H$^-$ ground state requires that an even number of photons excite the $^1D^e$ resonance, 10.873 eV above the ion ground state. Since the energy necessary to remove one electron from H$^-$ is only about 0.75 eV, the photon energy necessary to excite the $^1D^e$ by simultaneous absorption of two photons is also sufficient to detach an electron through single-photon absorption. Absorption of more photons than necessary to detach an electron from a negative
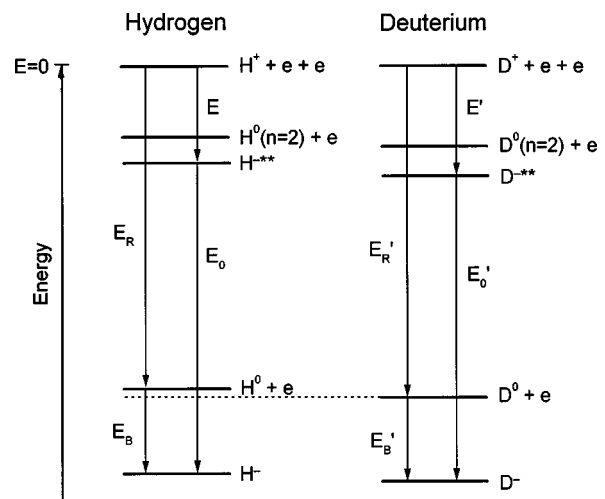

FIG. 1. A simplified energy-level diagram of negative hydrogen and negative deuterium (not to scale). The origin of the energy axis has been set to the three-body continuum in both isotopes.
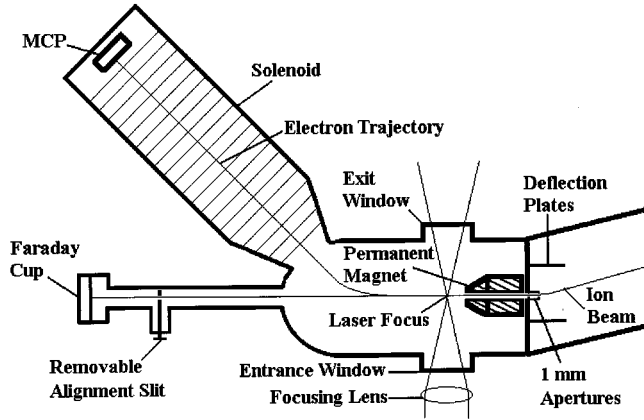
FIG. 2. A simplified schematic of the experimental setup (not to scale). A tunable uv laser is focused on a 1-mm-diam ion beam emerging from a cylindrical hole in a permanent magnet. Detached electrons are magnetically guided down a time-of-flight solenoid to a microchannel plate detector. Proper alignment was assured using a 1-mm-wide, 10-mm-high removable slit in front of the Faraday cup, 30 cm downstream from the magnet.

ion is referred to as excess photon detachment (EPD). The presence of the $^1D^e$ resonance increases the two-photon absorption rate by approximately two orders of magnitude [3]. Thus two-photon excitation of the $^1D^e$ is a unique example of final-state resonant EPD. Resonant EPD through an intermediate window resonance has been reported [4], as well as several observations of nonresonant EPD [5–8].

II. EXPERIMENTAL TECHNIQUES

The experimental setup is almost identical to the one described by Stinz *et al.* [1]. The essential feature is a collimated ion beam intersecting a focused pulsed laser beam at 90° (Fig. 2). The laser is linearly polarized in the direction of the ion velocity vector. The kinetic energy spectrum of the photodetached electrons is acquired using a magnetic time-of-flight (TOF) spectrometer adapted from a design by Kruit and Read [9] and modified by Kyrala [10]. In the two-photon absorption process described here, the kinetic energy of the detached electron in the rest frame of the ion beam is $T_e = 2h\nu - E_b$, where E_b is the binding energy of the negative ion species (H$^-$ or D$^-$) and $h\nu$ is the photon energy. The kinetic energy of an electron in the laboratory frame depends on its angle of ejection θ in the ion center-of-mass frame, where θ is measured from the ion velocity vector. In the laboratory frame, the electrons are ejected in a forward cone and are captured in a magnetic bottle that directs them to a microchannel plate (MCP) detector about a meter downstream. The yield Y of electrons at the detector as a function of time is given by

$$Y = \frac{1}{\sqrt{T_0 T_e}} \frac{md^2}{t^3} \frac{\sigma}{4} f(\theta),\qquad(1)$$

where T_0 is the kinetic energy of an electron traveling at the velocity of the ion beam, σ is the yield for a given photodetachment process, d the distance to the detector from the laser focus, and m the mass of the electron. Here $f(\theta)$, the angular distribution for two-photon detachment, is given by
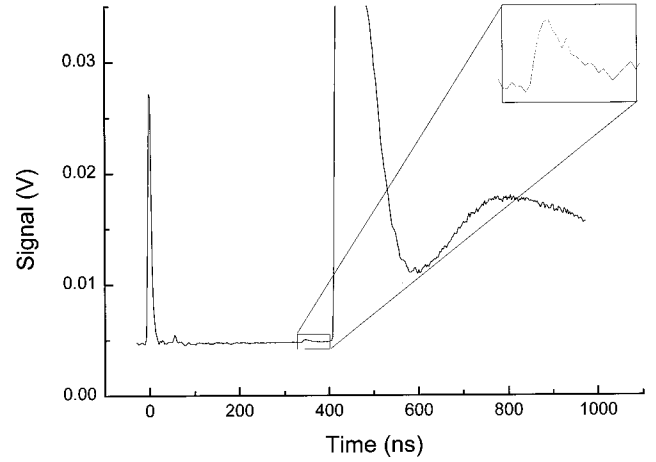

FIG. 3. A typical averaged oscilloscope trace. The spike at time zero is caused by uv photons produced by the laser. The large feature is the one-photon signal. Note that its leading peak, near 500 ns, is clipped by the oscilloscope. The smaller feature in the inset is the leading edge of the two-photon signal.

$$f(\theta) = [1 + \beta_2 P_2(\cos\theta) + \beta_4 P_4(\cos\theta)].\qquad(2)$$

The parameters β_2 and β_4 are referred to as *asymmetry parameters*, while P_2 and P_4 are Legendre polynomials. Because the kinetic energy T_{lab} in the laboratory frame is related to the angle of ejection θ according to

$$T_{\text{lab}} = T_0 + T_e + 2\sqrt{T_0 T_e}\cos(\theta),\qquad(3)$$

the angular distribution of Eq. (1) can be written as a function of time using the substitution

$$\cos(\theta) = \frac{md^2/2t^2 - (T_e + T_0)}{2\sqrt{T_e T_0}}.\qquad(4)$$

Since the ions in our experiment are initially in the $^1S^e$ ground state, photodetached electrons will be ejected as a P wave ($\beta_2 = 2$, $\beta_4 = 0$) for the single-photon process or a mixture of a D wave ($\beta_2 = 10/7$, $\beta_4 = 18/7$) and an S wave ($\beta_2 = \beta_4 = 0$) for two-photon detachment. One expects that at the peak photon energy of the $^1D^e$ resonance, photodetached electrons will be distributed primarily as a D wave. The leading edge (highest energy component) of the much weaker two-photon signal can be observed in the TOF spectrum as a small but distinctive peak appearing just before the one-photon signal (Fig. 3). Most of the two-photon signal lies in the same time region as the much larger one-photon signal and is obscured by it. Stinz *et al.* [1] demonstrated that this two-photon signal observed at the predicted photon energy of the $^1D^e$ is consistent with a resonance of D symmetry, although the actual asymmetry parameters were not reported.

H$^-$ or D$^-$ ions were generated by a Penning surface-plasma source and formed into a beam by a high-voltage extractor plate and a solenoid lens. The extractor plate voltage was varied to produce beam velocities βc between $0.0054c$ and $0.0076c$. After passing through a 6 mm aperture and two 1 mm apertures, the final ion current in the interaction region, which was monitored by a Faraday cup, was

~4 μA. A pulsed set of vertical deflector plates limited the ion current pulse to a duration of between 50 ns and 100 ns so that a minimal number of gas-stripped electrons were produced in the interaction region. The ion beam entered the interaction region through a concentric hole in a cylindrical samarium-cobalt permanent magnet (0.27 tesla) whose field lines merged downstream with those of a solenoid tube. Electrons ejected in the interaction region were guided by magnetic fields through the solenoid to a two-stage chevron-configuration MCP.

uv laser light near 228 nm was generated by sum-frequency mixing in a beta–barium borate (β-BBO) crystal of the Nd:YAG third harmonic and a tunable dye beam near 640 nm (DCM dye). After generating the third harmonic by mixing with the fundamental, the residual Nd:YAG second harmonic pumped the dye laser. The uv light had a 10 ns full width at half maximum (FWHM) Gaussian-like temporal profile, a nominally Gaussian spatial profile, and an energy of ~1 mJ per pulse. The beam was focused by a 10 cm focal length spherical lens into the interaction region about 3 mm downstream of the permanent magnet. The transverse dimensions of the laser focus were determined by scanning across the beam with a razor blade. In the interaction region the laser spot size was 13 μm thick (measured at the $1/e^2$ points) along the direction of the ion beam and 27 μm high in the vertical direction with a peak intensity of 9×10^9 W/cm^2. The dye laser wavelength was calibrated using a Fizeau wavemeter. The ions passed through the laser focus in a few tens of picoseconds.

The oscilloscope sampling rate of 1 GHz provides about 50 data points in the region of the two-photon peak. Resolution was limited primarily by the response of the MCP and the temporal profile of the laser pulse. Typically, at least 500 laser shots were averaged to produce an adequate two-photon signal, since normally only about one two-photon event was recorded for each laser shot at the peak resonance energy. Figure 3 is a typical averaged oscilloscope trace. The initial spike is caused by scattered uv laser photons incident on the detector. The structure with the large initial peak and smaller secondary peak is due to one-photon detachments, which have a P-wave angular distribution. The inset is a magnification of the much smaller two-photon detachment peak. Only those electrons ejected at small θ to the ion beam velocity are visible. The remaining two-photon electron pulses are buried in the one-photon signal.

III. MEASURING THE ISOTOPE SHIFT

Averaged TOF signal traces were obtained at a number of different dye-laser wavelengths. The wavelengths were chosen so that the two-photon energies of the sum-frequency generated light spanned a region centered on the $^1D^e$ peak. For each averaged trace, the visible portion of the two-photon signal (shown in the inset of Fig. 3) was integrated and plotted as a function of the two-photon energy. In this way we determined the spectrum of the resonance.

Figure 4 shows the integrated two-photon spectrum as a function of two-photon energy for typical H$^-$ and D$^-$ runs. The solid lines are fits to the data using the Beutler-Fano line shape [11]:

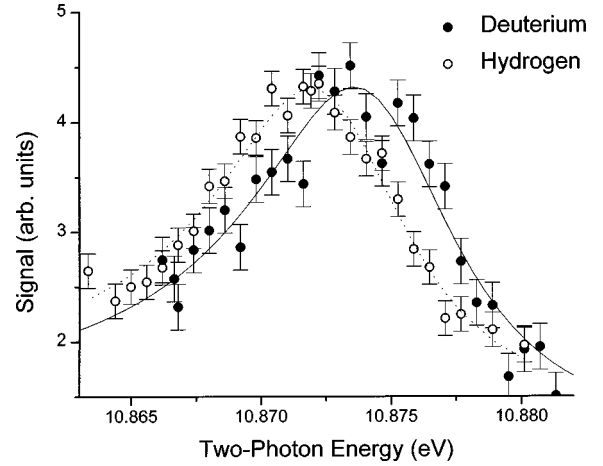FIG. 4. A plot of the integrated two-photon signal for H$^-$ and D$^-$ as a function of two-photon energy. The dotted line represents a fit of the Fano profile to the hydrogen data while the solid line represents a fit to the deuterium data. The peak shifts by ~2 meV with a change of isotopes. The isotope shift corresponds to ~20% the width of the peak.

$$\sigma(E) = \sigma_a \frac{(q+\epsilon)^2}{(1+\epsilon^2)} + \sigma_b \quad \text{with} \quad \epsilon = 2\frac{(E-E_0)}{\Gamma}, \quad (5)$$

where E_0 is the position of the resonance, Γ is the width, q is the shape parameter (line profile index), and σ_a and σ_b are relative cross sections. From an analysis of the theoretical form of the Fano shape parameter [12], we conclude that q should be independent of the nuclear mass to a very good approximation (i.e., the same for H$^-$ and D$^-$ resonances). Therefore the shape parameter was held at the same fixed value for fits to the spectra when comparing results for the two isotopes. Although our analysis shows that the fitted energy of the peak is strongly covariant with the value used for q (upper graph of Fig. 5), the energy difference in the peaks for the two isotopes is essentially independent of q. Our best estimate is $q = -5$. Stinz *et al.* [1] used $q = -8$ for their fits while theoretical data provided by Proulx and Shakeshaft [3] fit best with $q = -6.9$. More recent calculations by Sanchez *et al.* [13] indicate that the shape parameter should have an imaginary component, i.e., $q = -6.3 + i1.5$. Using the same theoretical data, we have determined that the Fano profile generated by $q = -6.6$ is practically indistinguishable from the complex-valued profile. Because of the strong covariance of E_0 and q, we have assigned an additional uncertainty of ± 1 meV to the position E_0 for both isotopes based on an estimated uncertainty in q of ± 2. The variation of Γ with q is negligible relative to the large uncertainties determined by the fitting algorithm. Most importantly, the lower graph of Fig. 5 demonstrates that the measured isotope shift appears to be almost completely independent of the choice of the shape parameter if we assume q is the same for both isotopes.

In a sensitive analysis such as we describe here, nonideal circumstances can distort the results. In what follows we will raise each possible source of systematic error, and discuss its impact on our conclusion. In this experiment the principal sources are mass-dependent departures of the intersection angle of the laser and ion beams from 90°.
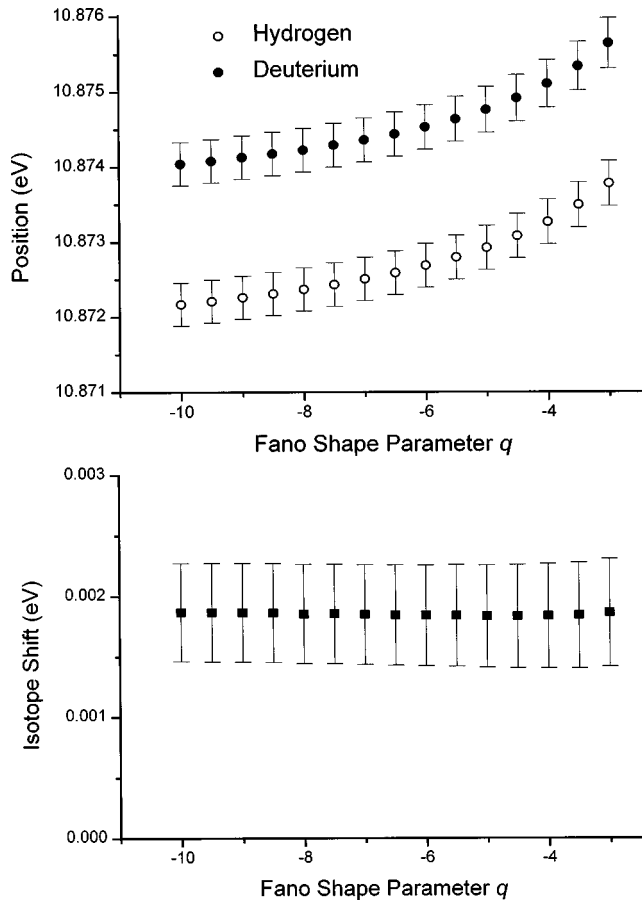
FIG. 5. The upper graph shows the variation of the position E_0 as a function of the Fano shape parameter q for the two isotopes. The lower graph indicates that the isotope shift does not vary appreciably with q.

Precision estimates of the position of the $^1D^e$ resonance in H^- and D^- must take into account possible inadvertent deviations of the angle of intersection from 90°. Although the ion velocity βc is too small to cause a measurable transverse Doppler shift of the photon energy, any deviation, α, of the laser beam from 90° to the ion-beam direction will cause a longitudinal Doppler shift $\Delta E = \beta E_0 \sin \alpha$, where E_0 is the two-photon energy. This Doppler shift can be a significant source of systematic error when measurements of the order $\Delta E/E = 10^{-5}$ are being made. The angle α, if it remains constant, can be determined indirectly by measuring the position E_0 of the resonance at several ion beam velocities and fitting the positions to a linear function of β. However, α may not be constant from run to run because the beam optics must be realigned each time the ion momentum (i.e., beam energy and isotope) is varied. To circumvent this difficulty, we placed a 1 mm slit 30 cm downstream of the permanent magnet, just before the Faraday cup. By adjusting the final set of deflector plates to align the beam with the slit, the intersection angle between the beams could be reproduced with an accuracy of 0.6 mrad, neglecting magnetic deflections from the permanent magnet to the final slit.

A more subtle variation in α results from variations in the ion velocity due to magnetic deflections along its trajectory. These deflections can result from the relatively large magnetic fields present in the region of the permanent magnet.

The experiment was designed so that the ions enter the interaction region along the central axis of the permanent magnet, in which case the magnetic field is entirely parallel to the ion beam velocity. However, ions that are not aligned along the z axis of the permanent magnet may be magnetically deflected, particularly at the laser focus where the magnetic field reaches a local maximum. If the deflection is in the plane of intersection of the laser and ion beams (which is the case when the ion beam is vertically misaligned), an additional Doppler shift will result. The total Doppler shift, including the linear effect described in the preceding paragraph, is given by

$$\Delta E = E_0 \left[\beta \sin \alpha + \frac{e}{(M+2m)c} \int B_\perp ds \right], \quad (6)$$

where e is the electron charge, c the velocity of light, M the nuclear mass, and $B_\perp$ the component of the magnetic field normal to the plane of intersection. The integration is over the ion trajectory from the entrance of the interaction region to the laser focus. The second term of Eq. (6) is an approximation relying on the assumption that the transit time of the ion in the magnetic field is much shorter than the gyration frequency. The equation is presented for the convenience of the reader. In actuality, our numerical calculations took into account the full equations of motion for an ion in a magnetic field. In general, then, one must have information on the initial conditions of the ion, particularly the vertical component of the velocity, in order to calculate the Doppler shift.

For a perfectly aligned system, the vertical deflector plates should be set to zero voltage during the 50–100 ns ion pulse. We found, however, that the plates had to be set to a small, nonzero voltage during the pulse to successfully direct the ion beam into the interaction region. Furthermore, the voltage was dependent on the ion momentum, suggesting that the vertical deflector plates were correcting for some systematic misalignment upstream. From the voltages on the plates, we were able to calculate the initial vertical angle of the ions with respect to the z axis of the permanent magnet as they entered the interaction region. Numerical calculations of the ion trajectory as it passed through the magnet and into the laser focus allowed us to estimate the Doppler shift. The resulting corrections to the resonance energies were generally small, the largest being $\delta E = -0.14 \pm 0.30$ meV for H^- at a velocity $\beta c = 0.0062c$. The net effect of the magnetic deflection was to decrease the apparent isotope shift by ~ 0.2 meV. We also studied the magnetic deflection induced by the TOF solenoid (which is two orders of magnitude weaker than the permanent magnet) and determined that it had an insignificant effect on the measured isotope shift.

Sixteen photon energy scans of the $^1D^e$ resonance in H^- and D^- were made using the 1 mm slit 30 cm downstream of the permanent magnet for alignment. A photon energy scan is constructed from a set of electron TOF spectra taken for series of photon energies spanning the range where the resonance is expected to reside. For each TOF spectrum, the integral of the forward, two-electron peak is computed and normalized to the beam current and the laser intensity; this two-photon yield vs the corresponding photon energy is termed a ''photon-energy scan.'' Of these 16, four were cut from the final set of data for having signal-to-noise ratios
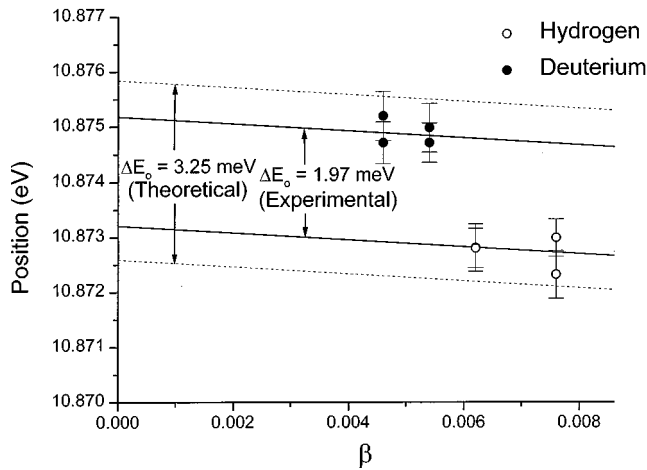
FIG. 6. The positions of the final set of eight data runs are plotted as a function of ion beam velocity. The solid lines represent the best-fit Doppler shift, which is a linear function of β. The dashed lines represent the best fit using the theoretical value of the isotope shift.

less than 1 or inordinately large backgrounds (twice the level of a typical scan) or both. Three sets of two scans taken contiguously were averaged to reduce the statistical spread in the data. The final set of eight scans, four H$^-$ scans and four

D$^-$ scans, were fit to a Fano profile with constant shape parameter as described above. Constant error bars were assigned to the data points based on a multiple of the expected Poisson uncertainty at the peak of the resonance, i.e., $\delta \propto V/\sqrt{N}$, where V is the maximum measured signal. The multiplicative factor was found to be approximately 1.6 by comparing the statistical spread of data points acquired in two consecutive resonance scans with the Poisson uncertainty. The additional uncertainty was probably due to random fluctuations in the laser intensity. In addition, the nonlinear crystal was retuned by hand as the dye wavelength was varied, leading to some variation in the average laser intensity. There is, however, no reason to expect this latter source of error to be proportional to the Poisson uncertainty.

The final positions of the peaks and the isotope shift were determined by plotting E_0 as a function of β (Fig. 6) for the reduced set of eight runs. After correcting the E_0's for the second term of Eq. (7), the contribution from the first term was determined by fitting the data to a function of three parameters: (i) the position of the $^1D^e$ peak in H$^-$, (ii) the Doppler shift angle α, and (iii) the isotope shift. The deviation of the intersection angle from 90° was found to be small, i.e., $\alpha = -6 \pm 22$ mrad. The positions and widths resulting from the fit are shown in Table I along with other experimental and theoretical values [1,3,13–28]. We report an isotope shift of 1.97 ± 0.53 meV with respect to the

TABLE I. Positions and widths of the $^1D^e$ resonance.

H$^-$	Year	Position (eV) [c]	Width (eV)
This work (experimental) [a]	1997	10.8732 ± 0.0027	0.0089 ± 0.0012
Chen (theoretical)	1997	10.8732	0.008651
Ho (theoretical)	1995	10.87291	0.008601
Sanchez, Martin, and Bachau (theoretical)	1995	10.8755	0.00889
Stinz et al. (experimental) [b]	1995	10.872 ± 0.002	0.0105 ± 0.0010
Proulx and Shakeshaft (theoretical)	1992	10.877	0.0096
Bhatia and Ho (theoretical)	1990	10.87304 ± 0.00004	0.008613 ± 0.000027
Scholz, Scott, and Burke (theoretical)	1988	10.8739	0.00881
Pathak, Kingston, and Berrington (theoretical)	1988	10.875	0.0088
Warner et al. (experimental)	1986	10.869 ± 0.0013	0.006 ± 0.002
Callaway (theoretical)	1978	10.8735	0.00872
Lipsky, Anania, and Conneely (theoretical)	1977	10.8747	
Bhatia and Temkin (theoretical)	1975	10.8727	10.0
Register and Poe (theoretical)	1975	10.8759	0.0090
Sanche and Burrow (experimental)	1972	10.882 ± 0.010	0.0073 ± 0.002
Bhatia (theoretical)	1972	10.86912	0.00100
Seiler, Oberoi, and Callaway (theoretical)	1971	10.914	0.00774
Ormonde, McEwen, and McGowen (experimental)	1969	10.88 ± 0.015	
Taylor and Burke (theoretical)	1967	10.873	0.0088
Burke, Ormonde, and Whitaker (theoretical)	1967	10.873	0.0088
D$^-$			
This work (experimental) [a]	1997	10.8752 ± 0.0027	0.0087 ± 0.0009
Isotope shift: [d] 2.0 ± 0.5 meV			

[a]$q = -5(2)$.
[b]$q = -8(2)$.
[c]The reduced Rydberg was used to convert to electron volts.
[d]Measured from the negative ion ground state.

negative-ion ground state. The isotope shift has been conveniently rounded to 2.0 ± 0.5 in Table I and the abstract, although all three significant digits were retained in calculating the mass polarization below. Within our uncertainty the resonance width is not isotope dependent; the difference in width between the two isotopes (hydrogen and deuterium) was found to be 0.2 ± 1.4 meV.

The internal kinetic energy of a three-body system is given by

$$T = \left[\frac{1}{2m} + \frac{1}{2M} \right] (p_1^2 + p_2^2) + \frac{\vec{p}_1 \cdot \vec{p}_2}{M}, \qquad (7)$$

where, for H^-, M is the proton mass. The final term, often referred to as *mass polarization* or *specific mass shift*, describes the portion of the Hamiltonian that is dependent on correlations of the electron momenta. Recently, several unpublished calculations of the mass-polarization contribution to the $^1D^e$ have been made. Chung [29] calculates a mass polarization of -0.103 meV, while Lindroth [30] and Ho [31] obtain the values -0.093 meV and -0.095 meV, respectively.

As we demonstrate below, our results indicate that the mass-polarization correction to the $^1D^e$ state is positive and somewhat larger than predicted. Figure 1 shows some relevant energy levels in H^- and D^- relative to the three-body continuum energy. Since D^- is more tightly bound than H^- by $E_B - E_{B'} = 0.40 \pm 0.08$ meV [32] and D^0 is more tightly bound than H^0 by $E_R - E_{R'} = 3.70$ meV [33], the shift with respect to the three-body continuum is $E - E' = 2.13 \pm 0.54$ meV. The virial theorem, $\langle T \rangle = -E$, indicates that $\langle T \rangle = E_B + E_R - E_0 = 3.480$ eV for hydrogen ions in the $^1D^e$ state. Here $\langle T \rangle$ is approximated by neglecting the last term of Eq. (7). The reduced mass portion of the isotope shift is

$$\Delta E = \langle T \rangle \left(\frac{\mu_D}{\mu_H} - 1 \right), \qquad (8)$$

accounting for 0.95 meV of the observed shift. Neglecting the volume shift (which is of the order of a neV [34]), the difference is the mass-polarization energy correction for the two isotopes:

$$\frac{\langle \vec{p}_1 \cdot \vec{p}_2 \rangle_H}{M} - \frac{\langle \vec{p}_1 \cdot \vec{p}_2 \rangle_D}{2M} = 1.18 \pm 0.54 \ \text{meV}. \qquad (9)$$

Assuming $\langle \vec{p}_1 \cdot \vec{p}_2 \rangle$ to be the same for the two isotopes, we conclude that mass polarization shifts the $^1D^e$ resonance in H^- by 2.4 ± 1.1 meV. Our measured value is thus 2.3 standard deviations from the theoretical prediction.

Two possible systematic interpretations for the discrepancy between our experimental results and theory have been considered: (i) the uncertainties in the data were underestimated and (ii) the ion beam optics were misaligned. Some evidence that the error bars were too small was obtained by comparing the statistical spread with the calculated error bars of Fig. 6. The standard deviation of the measured positions of the $^1D^e$ in H^- and D^- was about 60% larger than the quadrature sum of the uncertainties computed by the fitting algorithm, which were used above in the calculation of the isotope shift. This difference could be corrected by increasing the error bars used for the photon-energy scans by only 25%, which is difficult to justify given the limited amount of redundant data available. Second, a misalignment of the ion beam could result in a magnetic deflection, and thus a Doppler shift, that would be more significant for H^- than for D^-, resulting in a net systematic isotope shift. Fortunately, the two 1 mm apertures just before the interaction region are separated by 4 cm, which limits any possible misalignment to 25.3 mrad relative to the z axis of the permanent magnet. This corresponds to an additional isotope shift of at most 0.4 meV. The maximum systematic effect on the mass-polarization term in this resonance in hydrogen is thus about 0.8 meV. To summarize, our result for the mass-polarization term for the lowest $^1D^e$ term in negative atomic hydrogen is 2.4 ± 1.1 (experimental) ± 0.8 (systematic) meV.

Because of the relatively large experimental uncertainty and possible systematic error, we cannot regard our experimental result to be in definitive disagreement with theory. We believe, however, that this result should serve as a stimulus for a more precise measurement, for which this work could be a valuable guide.

IV. GENERALIZED ABSOLUTE CROSS SECTION MEASUREMENTS

The generalized cross section is based on the premise that the yields can be adequately described by lowest-order perturbation theory. In this case, with two-photon absorption, the generalized cross section is given by the ordinary cross section divided by the photon flux per unit area. The determination of this quantity requires detailed knowledge of the parameters of the overlap of the two interacting beams and rather elaborate modeling. Using a modified version of a model developed by MacKerrow and Bryant [35], we derived a formula to calculate the number of two-photon detachments per laser pulse (see Appendix). The mathematical description uses a thick-target approximation that includes depletion effects due to one-photon detachment. The most numerically efficient means of calculating the number of two-photon detachments from Eq. (A5) was to evaluate the x, y, and t integrals in a single quadrant. Also, improper integrals were truncated at twice the $1/e^2$ half-width, i.e.,

$$N_{d2} \approx 8 \frac{\sigma_2}{\beta c} \int_0^{2\tau} \int_{-2w_{z0}}^{2w_{z0}} \int_0^{2w_{y0}} \int_0^{2\rho_0} dx \ dy \ dz \ dt$$

$$\times F^2(x,y,z,t) J(x,y)$$

$$\times \exp\left(-\frac{\sigma_1}{\beta c} \int_{-\infty}^z dz' F(x,y,z',t) \right). \qquad (10)$$

Here σ_1 is the one-photon absolute cross section, and σ_2 is the generalized absolute cross section for two-photon detachment. The ions are assumed to be propagating along the z axis at velocity βc. The $1/e^2$ half-widths of the laser focus along the y and z axes are represented by w_{y0} and w_{z0}, respectively, while ρ_0 is the $1/e^2$ half-width of the ion beam and τ the temporal $1/e^2$ half-width of the laser pulse. In our calculations, the photon flux density F and the ion number current per unit area J were assumed to be Gaussian distributions.

To evaluate Eq. (10), no less than nine independent experimental parameters had to be determined in addition to σ_2. We compared predictions of Eq. (10) with the measured number of two-photon detachments at different laser intensities and found that the predicted variation with intensity was approximately linear and consistent with our data. The generalized absolute cross section was estimated by adjusting σ_2 until we obtained an optimum least-squares fit to the data. Error bars were assigned by adjusting each experimental parameter by one standard deviation and recomputing σ_2. In this way the rms deviation of the generalized cross section was computed for each parameter and summed to produce a total rms deviation.

Our results indicate that at the peak of the $^1D^e$, the generalized absolute cross section is $3.2^{+1.8}_{-1.2} \times 10^{-49}$ cm^4 s, or 420^{+240}_{-160} Γ/I^2 (a.u.), in approximate agreement with the theoretical value of 703 Γ/I^2 calculated by Sanchez et al. [13]. Proulx and Shakeshaft [3] obtain a similar value of ~ 710 Γ/I^2. The fact that our experimental value is somewhat smaller than the theoretical predictions may be the result of imperfect beam alignment or the use of laser wavelengths that are slightly off resonance.

A search was made for the second recursion of the $^1S^e$ resonance below the $N=2$ threshold and three-photon EPD. Neither process was observed. We were, however, able to assign an upper limit to the generalized absolute cross section for these two processes by comparing the noise level of our data with the size of the $^1D^e$ peak. The second $^1S^e$ is bounded by 2.8×10^{-49} cm^4 s, which disagrees with the calculations of Purvis et al. [36], who predict that the second $^1S^e$ has a larger cross section than the $^1D^e$. Three-photon EPD is bounded by 3.1×10^{-78} cm^6 s^2; no theoretical predictions exist at the photon energies used in our experiments.

Finally it should be mentioned that the absolute cross section for one-photon photodetachment, σ_1, was not measured. Because of the large number of electrons incident on the MCP, gain saturation effects distorted the signal. The gain of an MCP in pulsed-mode operation (where the duration of the measured signal is much smaller than the internal resistor-capacitor time constant of the MCP) is given by a particularly simple formula [37]:

$$g_c = g_0 \frac{\ln(1+\alpha q_0)}{\alpha q_0}, \qquad (11)$$

where g_0 is the unsaturated gain, q_0 the input charge, and α is a parameter we will call the *saturation coefficient*. Using a theoretical absolute one-photon cross section from Broad and Reinhardt [38] and calculating the predicted number of one-photon detachments from Eq. (A2), we were able to estimate the gain saturation coefficient for our particular MCP. We obtained $\alpha = (1.25 \pm 0.15) \times 10^{16}$, which agrees well with other values found in the literature [37,39].

V. ANGULAR DISTRIBUTION MEASUREMENTS

Theoretical predictions indicate that the asymmetry parameters of Eq. (1) vary significantly with photon energy in the region of doubly excited resonances [40]. In order to test this prediction, we analyzed 122 TOF spectra acquired at various photon energies in the region of the $^1D^e$. Using a
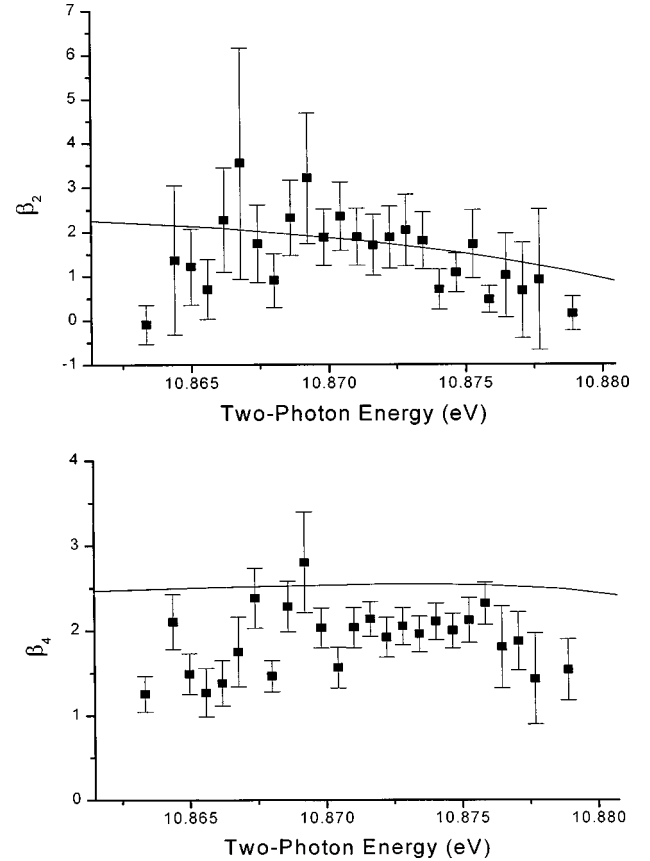

FIG. 7. The asymmetry parameters β_2 and β_4 as a function of two-photon energy. The solid lines represent calculated theoretical values.

computer-generated model to fit Eq. (1) to the TOF spectra, the asymmetry parameters were determined for a number of different photon energies. The results are plotted in Fig. 7 along with theoretical data from Ref. [40]. Each data point represents the weighted average of at least five separate measurements. Although β_4 is not predicted to vary significantly in this region of the photodetachment spectrum, theory indicates that β_2 should decrease with increasing photon energy. There appears to be some evidence for this conclusion in our data. Unfortunately, there is no way to exclude the possibility that the asymmetry parameters assigned by the fitting algorithm decrease systematically with the size of the two-photon signal, particularly far from resonance where the signal-to-noise ratio falls below 1.

We also determined the asymmetry parameters at the peak of the $^1D^e$. Only the 25 TOF spectra acquired at photon energies within ~ 1 meV of the peak were included in the analysis. Because the majority of the asymmetry parameters appeared to be normally distributed, they were plotted in histograms using a bin size of 0.5. By fitting Gaussian curves to histograms, we obtained values of 1.9 ± 1.2 and 2.21 ± 0.45 for β_2 and β_4, respectively. The ellipse of concentration for the asymmetry parameters is shown in Fig. 8 along with the experimental data points generated by the fitting algorithm. The wedge-shaped contour defines the region of physically allowed parameter space, which is determined from the condition that the photodetachment yield remain positive for all angles [41]. Because of the occasional poor convergence of the fitting algorithm, a larger number of out-
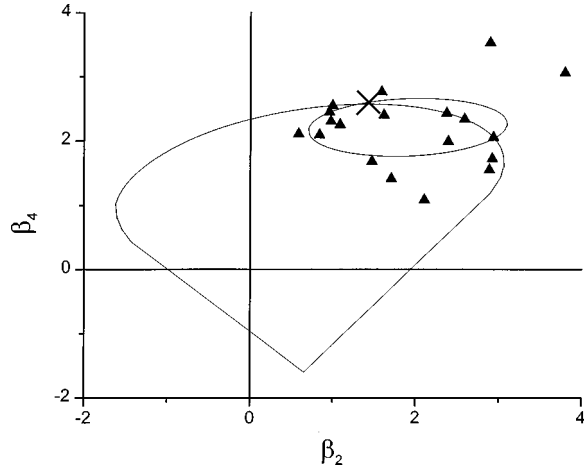
FIG. 8. The ellipse of concentration for the asymmetry parameters is represented along with the data points generated by the fitting algorithm. The region of parameter space containing physically allowed values is bounded by the wedge-shaped contour. The position of a pure D wave in parameter space is represented by an X. Note that six data points are beyond the boundaries of the figure.

liers were generated than one would expect from a normal distribution. In fact, only 32% of the data points fall within the ellipse of concentration. However, the method of fitting a Gaussian curve to a histogram reduces considerably the statistical weight of any outliers present in the data. Thus, if we ignore the eight data points that are well beyond the region of physically allowed values (six of which are also beyond the boundaries of the figure), we see that 53% of the remaining data fall within the ellipse of concentration, which is more consistent with the 68% one would expect from a normal distribution. Finally, we note that the values obtained for the asymmetry parameters are consistent with $\beta_2 = 10/7$ and $\beta_4 = 18/7$, which are the values one would expect for pure D-wave photodetachment.

VI. CONCLUSION

We have measured the isotope shift of the $^1D^e$ resonance of H^-, from which we have estimated the magnitude of the mass polarization effect using simple virial theorem arguments. Our results indicate that the mass polarization may be larger than the theoretical predictions. We cannot, however, consider the disagreement with theory definitive because of the possibility of systematic effects. The position of the $^1D^e$ resonance in H^- is in excellent agreement with theoretical calculations and previous experimental results. The widths are also in agreement, and no isotope effects beyond the energy shift were observed. The two-photon resonance EPD process was studied in detail, and the asymmetry parameters of the angular distribution were found to be in agreement with D-wave photodetachment. The measured generalized absolute cross section at the peak of the $^1D^e$ is somewhat smaller than theoretical predictions. Considering the large number of independent parameters involved in the cross-section calculation, the agreement with theory is surprisingly good.

APPENDIX: MODELING CROSSED-BEAM GEOMETRIES

In the thick-target approximation, depletion of the target ions has a significant effect on the total number of detachments. One must therefore define the probability of an ion surviving one-photon detachment to a position x,y,x at time t, i.e.,

$$P_{s1}(x,y,z,t) = \exp\left(-\frac{\sigma_1}{\beta c}\int_{-\infty}^{z} dz' F(x,y,z',t) \right), \quad (A1)$$

where σ_1 is the one-photon absolute cross section, F the photon flux density, and βc the ion velocity. Here, we have defined the origin to be at the intersection of the laser and ion beams, while the z axis is defined to be parallel to the ion beam direction. An implicit assumption in Eq. (A1) is that the ions pass through the laser focus in a time much shorter than the duration of the laser pulse. From the probability of survival, one can derive an expression for the number of one-photon detachments:

$$N_{d1} = \int_{-\infty}^{\infty}\int_{-\infty}^{\infty}\int_{-\infty}^{\infty} dx\, dy\, dt [1 - P_{s1}(x,y,z\rightarrow\infty,t)] J(x,y),$$
$$(A2)$$

where J is the number current of ions per unit area.

Except for cases where the photon flux density is very large, depletion due to two-photon detachment is negligible. For ions surviving one-photon detachment, one can therefore use a thin-target approximation to calculate the two-photon detachment probability. Thus, the probability of two-photon detachment per infinitesimal distance of penetration dz into the laser focus is given by

$$\frac{dP_{d2}(x,y,z,t)}{dz} \approx \frac{\sigma_2}{\beta c} F^2(x,y,z,t) P_{s1}(x,y,z,t), \quad (A3)$$

where σ_2 is the generalized absolute cross section for two-photon absorption. The total number of two-photon detachments is then

$$N_{d2} \approx \frac{\sigma_2}{\beta c}\int_{-\infty}^{\infty}\int_{-\infty}^{\infty}\int_{-\infty}^{\infty}\int_{-\infty}^{\infty} dx\, dy\, dz\, dt$$
$$\times F^2(x,y,z,t) J(x,y,z,t)$$
$$\times \exp\left(-\frac{\sigma_1}{\beta c}\int_{-\infty}^{z} dz' F(x,y,z',t) \right). \quad (A4)$$

At this point, one need only find an expression for the photon flux F and the ion number current per unit area J. In many cases, F and J can be approximated by Gaussian distributions. For a typical, low-divergence ion beam, the number current per unit area can be expressed as

$$J(x,y) = \frac{2}{\pi} \frac{I}{q\rho_0^2} \exp\left[\frac{-2(x^2+y2)}{\rho_0^2}\right], \qquad (A5)$$

where ρ_0 is the $1/e^2$ half-width of the beam, q the charge per ion, and I the current. A similar Gaussian distribution can be defined for the laser. If x is defined to be along the axis of the laser beam, the expression for the photon flux is

$$F(x,y,z,t) = \left(\frac{2}{\pi}\right)^{3/2} \frac{N_{ph}}{\tau w_y(x) w_z(x)}$$
$$\times \exp\left(\frac{-2t^2}{\tau^2}\right) \exp\left(\frac{-2y^2}{w_y(x)^2}\right) \exp\left(\frac{-2z^2}{w_z(x)^2}\right).$$
$$(A6)$$

Here N_{ph} is the number of photons per laser pulse and τ is the temporal $1/e^2$ half-width. The spot sizes in the y and z directions are $w_y(x)$ and $w_z(x)$, respectively. For long focal geometries, the expansion of the laser beam on either side of the focus is negligible, and the spot sizes can be approximated by constants w_{y0} and w_{z0}. For beams that are more tightly focused, the full x dependence of the spot sizes must be made explicit, i.e.,

$$w_y(x) = w_{y0}\left(\frac{x_{y0}^2 + x^2}{x_{y0}^2}\right)^{1/2} \qquad (A7)$$

and

$$w_z(x) = w_{z0}\left(\frac{x_{z0}^2 + x^2}{x_{z0}^2}\right)^{1/2}, \qquad (A8)$$

where x_{y0} and x_{z0} are the Rayleigh ranges in the y and z directions, respectively. For a cylindrically symmetric laser focus, the y and z directions will be indistinguishable. A more detailed derivation of the above equations appears in Ref. [2].

---

[1] A. Stinz et al., Phys. Rev. Lett. **75**, 2924 (1995).

[2] D. C. Rislove, Ph.D. dissertation, University of New Mexico, Albuquerque, NM, 1997.

[3] D. Proulx and R. Shakeshaft, Phys. Rev. A **46**, R2221 (1992).

[4] H. Stapelfeldt and H. K. Haugen, Phys. Rev. Lett. **69**, 2638 (1992).

[5] M. D. Davidson, H. G. Muller, and H. B. van Linden van den Heuvell, Phys. Rev. Lett. **67**, 1712 (1991).

[6] H. Stapelfeldt et al., Phys. Rev. Lett. **67**, 1731 (1991).

[7] C. Blondel et al., J. Phys. B **24**, 3575 (1991).

[8] X. M. Zhao et al., Phys. Rev. Lett. **78**, 1656 (1997).

[9] P. Kruit and F. H. Read, J. Phys. E **16**, 313 (1983).

[10] G. A. Kyrala and T. D. Nichols, Phys. Rev. A **44**, R1450 (1991).

[11] U. Fano, Phys. Rev. **124**, 1866 (1961).

[12] H. Friedrich, Theoretical Atomic Physics (Springer-Verlag, New York, 1990), Eq. (3.69), p. 137.

[13] The complex Fano shape parameter and additional data were supplied to us by F. Martin from I. Sanchez, F. Martin, and H. Bachau, J. Phys. B **28**, 2863 (1995).

[14] M.-K. Chen, J. Phys. B **30**, 1669 (1997).

[15] Y. K. Ho, Phys. Rev. A **52**, 375 (1995).

[16] A. K. Bhatia and Y. K. Ho, Phys. Rev. A **41**, 504 (1990).

[17] T. Scholz, P. Scott, and P. G. Burke, J. Phys. B **21**, L139 (1988).

[18] A. Pathak, A. E. Kingston, and K. A. Berrington, J. Phys. B **21**, 2939 (1988).

[19] C. D. Warner et al., J. Phys. B **19**, 3297 (1986).

[20] J. Callaway, Phys. Lett. **65A**, 199 (1978).

[21] L. Lipsky, R. Anania, and M. J. Conneely, At. Data Nucl. Data Tables **20**, 132 (1977).

[22] A. K. Bhatia and A. Temkin, Phys. Rev. A **11**, 2018 (1975).

[23] D. Register and R. T. Poe, Phys. Lett. **51A**, 431 (1975).

[24] L. Sanche and P. D. Burrow, Phys. Rev. Lett. **29**, 1639 (1972).

[25] G. J. Seiler, R. S. Oberoi, and G. Callaway, Phys. Rev. A **3**, 2006 (1971).

[26] S. Ormonde, J. McEwen, and J. W. McGowan, Phys. Rev. Lett. **22**, 1165 (1969).

[27] A. J. Taylor and P. G. Burke, Proc. Phys. Soc. London **92**, 336 (1967).

[28] P. G. Burke, S. Ormonde, and W. Whitaker, Proc. Phys. Soc. London **92**, 319 (1967).

[29] K. T. Chung (private communication).

[30] E. Lindroth (private communication).

[31] Y. K. Ho (private communication).

[32] K. R. Lykke, K. K. Murray, and W. C. Lineberger, Phys. Rev. A **43**, 6104 (1991).

[33] C. Wieman and T. W. Hänsch, Phys. Rev. A **22**, 192 (1980).

[34] E. E. Salpeter, Phys. Rev. **89**, 92 (1952).

[35] E. P. MacKerrow and H. C. Bryant, in Proceedings of the Fourth US/Mexico Symposium on Atomic and Molecular Physics, Queretero, Mexico, 1994, edited by I. Alvarez, C. Cisneros, and T. J. Morgan (World Scientific, Singapore, 1995).

[36] J. Purvis et al., Phys. Rev. Lett. **71**, 3943 (1993).

[37] L. Giudicotti et al., Rev. Sci. Instrum. **65**, 247 (1993).

[38] J. T. Broad and W. P. Reinhardt, Phys. Rev. A **14**, 2159 (1976).

[39] E. H. Eberhardt, IEEE Trans. Nucl. Sci. **NS-28**, 712 (1981).

[40] I. Sanchez, H. Bachau, and R. Martin, J. Phys. B **30**, 2417 (1997).

[41] C. Blondel and C. Delsart, Laser Phys. **3**, 699 (1993).